Why and How to Measure the Non-Metallized Contact Resistivity of a Passivating Contact

Andreas Fell
Fraunhofer Institute for Solar Energy Systems
Freiburg, Germany
andreas.fell@ise.fraunhofer.de

Christian Reichel
Fraunhofer Institute for Solar Energy Systems
Freiburg, Germany
christian.reichel@ise.fraunhofer.de

Tobias Fellmeth
Fraunhofer Institute for Solar Energy Systems
Freiburg, Germany
tobias.fellmeth@ise.fraunhofer.de

Christoph Luderer
Fraunhofer Institute for Solar Energy Systems
Freiburg, Germany
christoph.luderer@ise.fraunhofer.de

Frank Feldmann
Fraunhofer Institute for Solar Energy Systems
Freiburg, Germany
frank.feldmann@ise.fraunhofer.de

Martin Hermle
Fraunhofer Institute for Solar Energy Systems
Freiburg, Germany
martin.hermle@ise.fraunhofer.de

Stefan W. Glunz
Fraunhofer Institute for Solar Energy Systems
Freiburg, Germany
stefan.glunz@ise.fraunhofer.de

***Abstract* — When a silicon solar cell passivating contact is combined with a metal grid, the lateral resistance of the wafer and of the passivating contact layer, as well as their interface resistances, are decisive for a high fill factor (*FF*). A particular challenge for characterization and modelling arises for industrial bifacial TOPCon solar cells featuring fire-through metallization on the rear side, in which case three contact resistivities are of relevance: (i) the contact resistivity over the thin oxide under the metallization, (ii) the same in the non-metallized region, and (iii) the contact resistivity between the poly-Si and the metal. We show that a common approach to determine a single lumped contact resistivity via transfer length method (TLM) may result in large errors when predicting its influence on *FF*. We then present a new approach to determine the three contact resistivities via a modified TLM structure and fitting of Quokka3 simulations, which we call biTLM.**

I. Introduction

For locally contacted solar cells, the lateral conductivity is an important factor for high efficiencies. This lateral conductivity is given by the wafer itself and often in addition by a laterally conductive layer ("skin"). For most both-sides contacted solar cells the lateral conductivity of the skin on the front side is essential to allow a large finger pitch for minimizing shading losses and achieving a high fill factor *FF*. For the same reason the lateral conductivity is also important if employed on the rear side within bifacial cell concepts, which this work focuses on. For common bifacial industrial cell concepts (e.g. PERT), the lateral conductivity of the skin is achieved by high near-surface doping via thermal diffusion. Advanced cell concepts are replacing such diffusions by "passivating contacts" with lateral conductance, most prominently i) amorphous silicon (a-Si) with a transparent conductive oxide (TCO) in silicon heterojunction (SHJ) cells, and ii) thin oxide with relatively thick (100 nm – 250 nm) highly doped poly silicon (TOPCon). One important difference to common diffused skins is that additional interface resistances between the silicon wafer and the metallization occur. For SHJ this additional resistance is mainly arising from the intrinsic a-Si layer and the doped a-Si/TCO interface [1], and for the TOPCon structure from the thin oxide layer. These additional transport losses, which is here called a "skin resistivity", come in addition to the contact resistance between the skin and the metallization. A further complication arises for industrial-type TOPCon cells, meaning the use of fire-through metallization on a rear-side poly-silicon contact in a bifacial cell design: spiking of the metallization through the oxide most likely reduces the interface resistance over the oxide underneath the metallization [2], resulting in a total of three relevant contact resistivities: (i) bulk-skin metallized $\rho_{skin,met}$, (ii) bulk-skin non-metallized $\rho_{skin,nomet}$, and (iii) skin-metal ρ_{met}, see Fig. 1, all affecting the current transport losses, i.e. the *FF* of the solar cell.

When $\rho_{skin,nomet}$ is equal to $\rho_{skin,met}$, (and strictly speaking when also $J_{0,skin,nomet}$ is equal to $J_{0,skin,met}$) like e.g. for the HJT cell, we speak of a "true" passivating contact. In this case it is possible to determine both $\rho_{skin,met}$ and ρ_{met} by different test-structures, e.g. comparing a Cox-Strack measurement with a standard transfer-length-method (TLM) measurement [3]. Such methods, however, cannot directly determine the $\rho_{skin,nomet}$. One possibility for its determination is a comparison of a four-point-probe and inductive conductance measurement [4]. An analytical method similar to TLM has been presented in [5] to separate the aforementioned three contact resistivities for microelectronic applications. It, however, is not well applicable to industrial solar cell designs, due to the small metallization geometry required, and the simplification of the second layer (the bulk) to a lateral sheet conductance. In [6] a method for the discrimination of ρ_{skin} and ρ_{met} was presented via etching the poly-Si in between the metallization, and

subsequent fitting of Quokka3 device simulation, which is however impractical as a routine measurement.

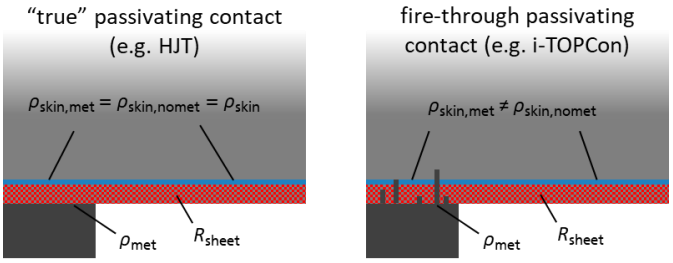

Fig. 1. Sketch of the (up to) three relevant contact resistivities for a laterally conductive passivating contact skin with a metal grid.

Due to the difficulties of determining the several contact resistivities, often a standard TLM measurement is performed, and the resulting contact resistivity is treated as a lumped value applied to ρ_{met} and assuming the skin resistivities as zero.

In this paper we firstly quantify the error of such a lumped TLM approach to predict the *FF* of a bifacial solar cell with a rear passivating contact via a Quokka3 simulation study. We then propose the biTLM method to determine the contact resistivities by measuring an easy-to-manufacture standard industrial TLM structure with and without full rear metallization, and fitting Quokka3 simulations to the measured resistances.

II. Quokka3 Simulations

In the following we use the software Quokka3 [7] to define 2D cross section of an *n*-type bifacial solar cell to simulate the fill-factor (FF), as well as of the corresponding TLM test structure to simulate the resistance as a function of distance, see Fig. 2. Quokka3 allows the definition of different metallized and non-metallized skin resistivities by creating a local skin aligned with the metallization, and also consider ρ_{met} between the skin and the metal fingers. It is thus able to correctly model the multidimensional current flow in the bulk, coupled via the contact resistivities with the skin layer and also the metal fingers. For the TLM structure simulations we use the resistive mode of Quokka3, in which solely majority carrier current transport is modelled while neglecting any semiconductor physics, resulting in a significant simplification of the simulation settings and in an increase of simulation speed suitable for experimental data fitting. Here, we focus on a typical industrial TLM structure, meaning a stripe cut out from the solar cell. The exemplary assumed bulk resistivity is 2 Ωcm and the passivating contact skin's sheet resistance *R*sheet 80 Ω, respectively.

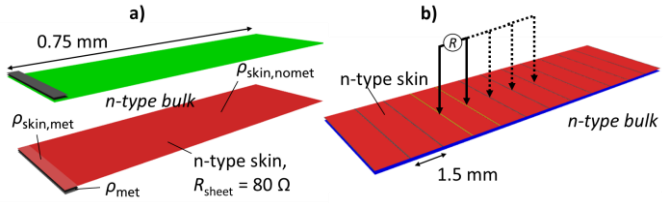

Fig. 2. Quokka3 simulation domains used in this work: a) unit-cell of a ~23.5% efficient bifacial solar cell with the passivating contact of interest on the rear side; b) corresponding TLM structure simulated using Quokka3's resistive mode.

Note that the simulation setup, and all findings of this paper, assume the contact resistivities to be ohmic. However, passivating contacts may be non-ohmic, e.g. caused by tunneling over the thin oxide. While Quokka3 is able to consider non-ohmic effects via an MIS model, this would add another dimension in complexity to the presented analysis and is not addressed in this paper. It is advisable to check for any non-ohmic effects experimentally to ensure the validity of this purely ohmic analysis.

III. TLM Error

For a simplified treatment of the situation, it would be desirable if the various contact resistivity effects could be lumped into a single value for ρ_{met}. For this to be useful, the ρ_{met} derived by the most common method for contact resistivity determination, namely TLM, should be able to approximately quantify the associated transport losses, i.e. the *FF* loss of the solar cell. In this section we test this by a simulation study using Quokka3. We simulate both the TLM structure and the "correct" solar cell *FF* with various values for the three contact resistivities. We then apply the classical TLM theory to extract a lumped "apparent" ρ_{met} from the simulated TLM measurement, which we subsequently insert into a second solar cell simulation assuming the other contact resistivities to be zero. The difference to the correct FF then quantifies the systematic error associated with this lumped TLM approach.

In Fig. 3 and Fig. 4 it can be seen that the apparent ρ_{met} extracted by TLM largely underestimates the contact resistivity related FF loss when $\rho_{skin,nomet}$ becomes significant, both for true ($\rho_{skin,met} = \rho_{no,met}$) and fire-through passivating contacts ($\rho_{skin,met} \neq \rho_{no,met}$). Only when $\rho_{skin,nomet}$ is negligible the *FF* loss is usefully accurate, notably despite the thick bulk still violating the TLM assumption of purely lateral current transport between the fingers. The derived apparent ρ_{met} represents the actual ρ_{met} when the latter is high (see second y-axis in Fig. 3), instead of being an effective parameter for all contact resistance related losses. In other words, the effect

of $\rho_{skin,nomet}$ on *FF* is missed out by the common TLM analysis.

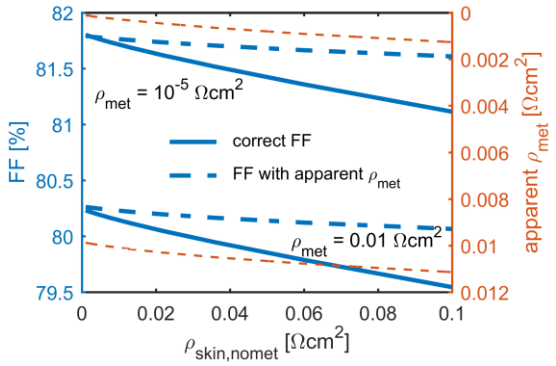

Fig. 3. FF error by extracting a lumped apparent ρ_{met} via TLM and using it to model the *FF* loss of the respective solar cell for a **true passivating contact** ($\rho_{skin,met} = \rho_{skin,nomet}$), for two cases for ρ_{met}.

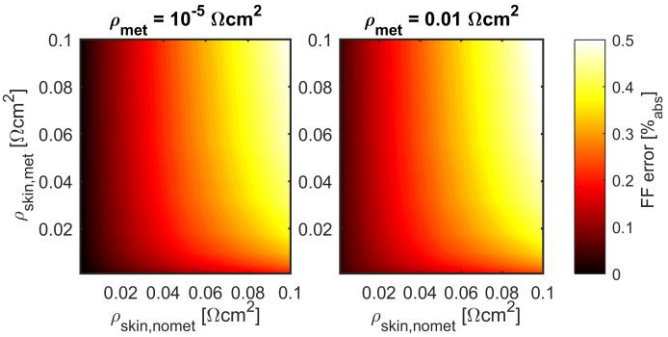

Fig. 4. *FF* error as in Fig. 3. for a **fire-through passivating contact** ($\rho_{skin,met} \neq \rho_{no,met}$)..

Notably, also for the case of a large *FF* error, i.e. a large $\rho_{skin,nomet}$, the measured resistance as a function of distance is still strongly linear, resulting also in an apparently very low error of the apparent ρ_{met}, see Fig. 5. This means that the systematic error from a non-negligible $\rho_{skin,nomet}$ is not obvious from the TLM measurement itself, which fosters the danger of misinterpretation.

An equivalent effect, but with even larger errors, is expected when the passivating contact of interest is applied to the front side of the solar cell, and / or forms a *pn*-junction instead of the investigated high-low junction.

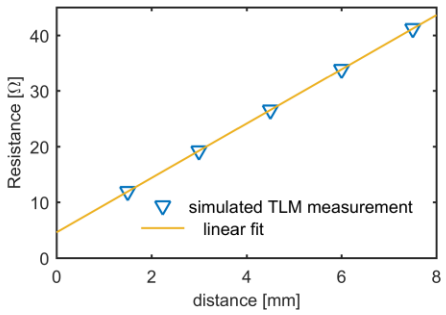

Fig. 5. Linear fit of simulated TLM measurement for the case of the largest *FF* error: $\rho_{skin,met} = \rho_{no,met} = 0.1$ Ωcm² and $\rho_{met} = 0.01$ Ωcm².

IV. biTLM METHOD

A. *Method description*

We propose to combine the standard TLM measurement of an unipolar sample and a measurement of an identical structure but with a full rear metallization. This substantially changes the current path from lateral current transport in the bulk and the skin to vertical current transport between the front and the rear. This results in (almost) a saturation of the measured resistance for larger distances, due to the very low lateral resistance of the metal, see Fig. 6. This second measurement is thus not only more, but importantly also differently sensitive to the contact resistivities of interest. The approach to determine the unknown parameters, namely R_{sheet}, ρ_{met}, $\rho_{skin,met}$ and $\rho_{skin,nomet}$, is to simulate the measurable resistance as a function of distance for those two structures with Quokka3 and perform a multivariate non-linear-least-squares (NLSQ) fit to the corresponding measured resistances. A benefit of rigorously fitting the unknown parameters against all available measurements simultaneously is that the NLSQ algorithm can provide meaningful confidence bounds. Those bounds also take into account parameter covariance, which is important for a many variable fit. Notably, the other device properties, in particular the bulk resistivity, need to be determined independently, as we found that using more fit parameters will result in strong covariance problems.

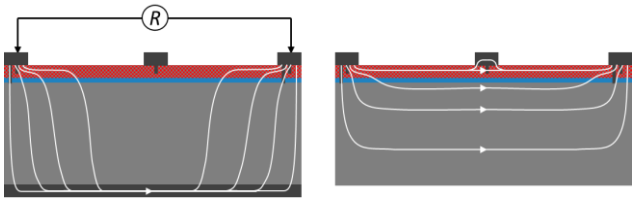

Fig. 6. Sketch of the two sample types: standard TLM structure (left), and the identical structure with full rear metallization (right).

B. *Results for industrial TOPCon (fire-through passivating contact)*

Here we present initial biTLM results for an industry-typical TOPCon TLM structure as sketched in Fig. 2 b), where the full area rear metallization was achieved with the same screen-printing process as at front side. The results in Fig. 7 show that R_{sheet} and a low upper bound for ρ_{met} are successfully determined. $\rho_{skin,nomet}$ has a significant error, while $\rho_{skin,met}$ could not be determined with useful accuracy. The reasons for the inaccuracies of this initial measurement are: i) the bulk resistivity (around 4 Ωcm) has not been measured accurately beforehand, and may well be different between the samples with and without rear metal; ii) the two sample types have been processed on different dates, making inconsistencies in sample properties likely. Furthermore, the accuracy can substantially be improved when using a smaller finger pitch.

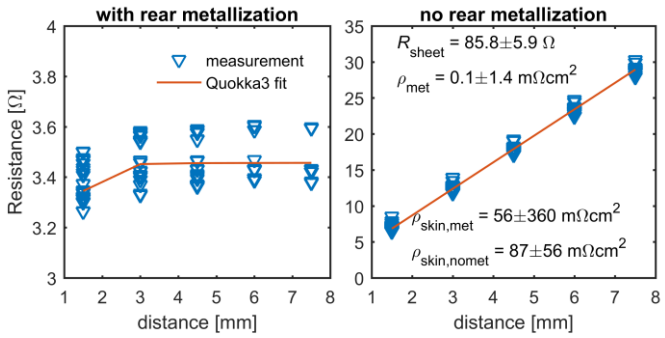

Fig. 7. Measurement data and fit result for an industry-typical TOPCon TLM structure with (left) and without full-rear metallization (right); resulting fit parameters are shown with the 95% confidence interval.

Notably, the inaccuracies of these initial measurements highlight one advantage of the rigorous multivariate NLSQ approach in giving also meaningful errors of the fit parameters. Potential alternative multi-step analysis based on analytical formulas may miss out for example on the important covariance errors, with the danger of misinterpreting the results with false high confidence. In other words, it is very valuable to know that in this case $\rho_{skin,met}$ could not be determined with suitable accuracy.

C. *Results for laboratory TOPCon (true passivating contact)*

We finally apply the new method to a true passivating contact, in this case a laboratory TOPCon layer with evaporated metallization similar as used in the record efficiency devices of Fraunhofer ISE [8]. By photolithography we create a Berger TLM structure [9]with much smaller distances compared to the industrial TLM structure, namely 10 µm to 120 µm. The metal pads are 2 mm long and 0.6 mm wide. We found that even for this relatively large ratio of pad length and gap size, the current flow through the perimeter of the structure significantly influences the resistances and thus fitting results. We address this by simulating a 3D domain covering two neighboring pads with a variable gap and including the perimeter region, see Fig. 8. We investigate both *p*-type and *n*-type TOPCon layers, using the same respective bulk doping type with a resistivity of ~1 Ω cm. The fitting procedure is adjusted to three fit parameters only, as for this true passivating contact there is only a single skin resistivity ρ_{skin}.

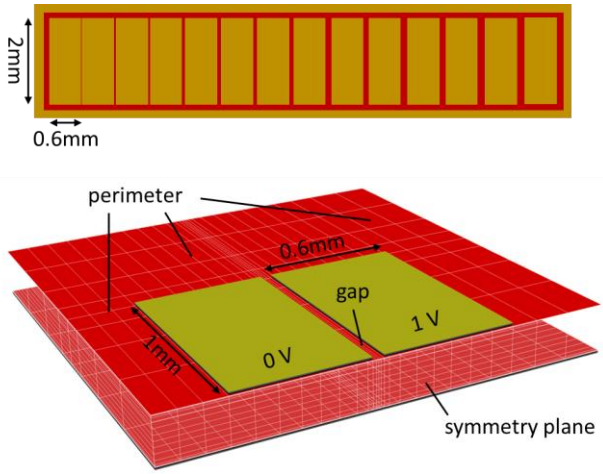

Fig. 8. Sketch (top) and half-symmetry Quokka3 3D solution domain (bottom) for the Berger TLM structure.

Fig. 9 and Fig. 10 show the results for *n*-type and *p*-type, respectively. In both cases the fit was successful in determining all unknown parameters with very satisfactory accuracy, meaning that in both cases the two contact resistivities are successfully discriminated by the new method. As expected, the contact resistances are lower for *n*-type, with a very low value < 1 mΩ cm² for ρ_{skin} and a slightly higher value for ρ_{met}. For *p*-type, both values are higher and similar.

Notably, the measured data points for the first gap size of 10 µm are a bit off, which is due to another edge effect being the first pad of the structure. This is not attempted to be resolved in the simulations, but we rather exclude the first gap size for the fit. Ideally one would simulate the full Berger structure in 3D to account for all those edge effects, potentially influencing the fit results. By a variation of the perimeter we found that this would mainly impact the derived sheet resistance towards higher values, but only marginally the contact resistivities.

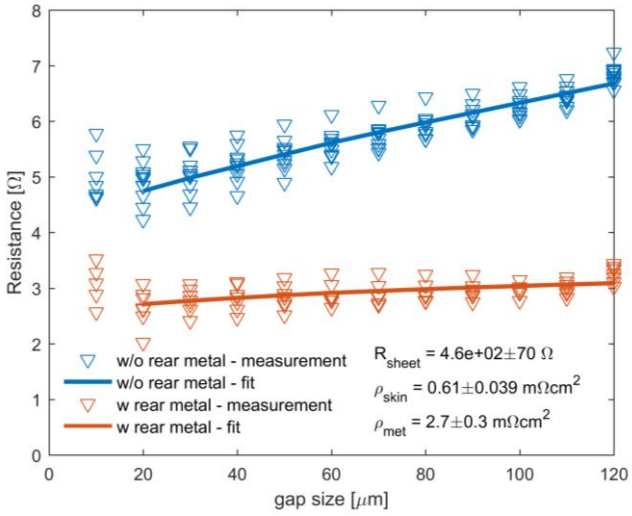

Fig. 9. Fitting results for the ***n*-type** laboratory TOPCon Berger structure.

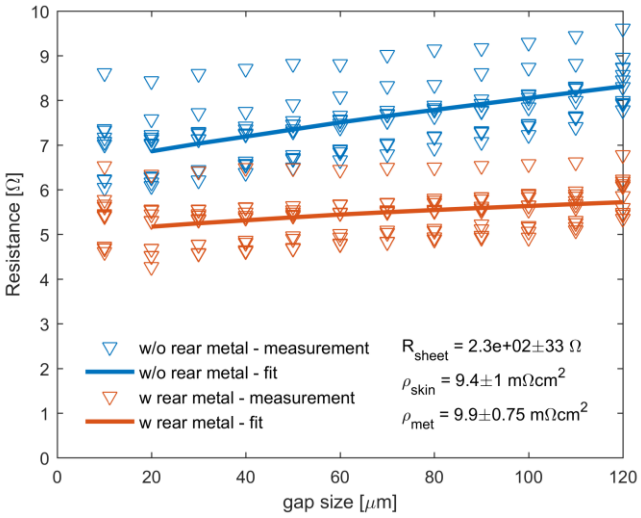

Fig. 10. Fitting results for the ***p*-type** laboratory TOPCon Berger structure.

V. Conclusions

We have shown that in the presence of a significant resistance between the bulk and the lateral transport layer of a passivating contact skin in the non-metallized region, the measurement of a single lumped contact resistivity via TLM may result in large errors when using it to predict the FF of a solar cell. Therefore, the characterization of all relevant contact resistivities is strongly desirable. For this we proposed the new biTLM method to measure a common TLM structure with and without full rear metallization and fit the measurements by Quokka3 simulations. The biTLM method was successfully applied on a laboratory TOPCon skin with evaporated metallization by accurately determining the contact resistivity between the bulk and the poly-Si, as well as the poly-Si and the metal. We also performed initial test on industrial TOPCon skin with fire-through metallization. This adds the complexity of the skin resistivity being likely different in the metallized and non-metallized area due to spiking, and also restricts the TLM structure to relatively widely spaced fingers for the ease of processing and measurement. While the fitting results on these initial experimental data show some significant uncertainties, due to a non-ideal experimental design, biTLM is shown to work in principle. In fact, a strength of the rigorous NLSQ fit becomes obvious in providing meaningful confidence bounds, which allowed the identification of the large parameter uncertainty. We are confident that with a proper experimental design the biTLM method is able to discriminate all relevant contact resistivities also for an industrial TOPCon structure with sufficient accuracy.

REFERENCES

[1] C. Luderer *et al.*, "Transport Losses at the TCO/a-Si:H/c-Si Heterojunction: Influence of Different Layers and Annealing," *IEEE J. Photovoltaics*, pp. 1–7, 2020.

[2] H. E. Çiftpınar *et al.*, "Study of screen printed metallization for polysilicon based passivating contacts," *Energy Procedia*, vol. 124, pp. 851–861, 2017.

[3] T. Gao *et al.*, "An industrially viable TOPCon structure with both ultra-thin SiOx and n+-poly-Si processed by PECVD for p-type c-Si solar cells," *Solar Energy Materials and Solar Cells*, vol. 200, p. 109926, http://www.sciencedirect.com/science/article/pii/S0927024819302478, 2019.

[4] U. Römer *et al.*, "Recombination behavior and contact resistance of n+ and p+ poly-crystalline Si/mono-crystalline Si junctions," *Solar Energy Materials and Solar Cells*, vol. 131, pp. 85–91, http://www.sciencedirect.com/science/article/pii/S0927024814003080, 2014.

[5] K.-C. Huang *et al.*, "A Transfer Length Model for Contact Resistance of Two-Layer Systems with Arbitrary Interlayer Coupling - Electron Devices, IEEE Transactions on," *IEEE Transactions on Electron Devices*, vol. 43, no. 5, pp. 676–684, 1996.

[6] G. Kökbudak *et al.*, "On the determination of the contact resistivity for passivating contacts using 3D simulations," in *34th European Photovoltaic Solar Energy Conference and Exhibition*, Amsterdam, 2017.

[7] A. Fell *et al.*, "The concept of skins for silicon solar cell modeling," *Solar Energy Materials and Solar Cells*, vol. 173, no. Supplement C, pp. 128–133, 2017.

[8] A. Richter *et al.*, "n-type Si solar cells with passivating electron contact: Identifying sources for efficiency limitations

by wafer thickness and resistivity variation," *Solar Energy Materials and Solar Cells*, 2017.

[9] H. H. Berger, "Contact Resistance and Contact Resistivity," (en), *J. Electrochem. Soc.*, vol. 119, no. 4, p. 507, https://iopscience.iop.org/article/10.1149/1.2404240/meta, 2019.